EUROPEAN JOURNAL OF PURE AND APPLIED MATHEMATICS
Vol. 17, No. 2, 2024, 1009-1028
ISSN 1307-5543 – ejpam.com
Published by New York Business Global

A Novel Fractional Edge Detector Based on Generalized Fractional Operator

Diaa Eldin Elgezouli[1], Mohamed A. Abdoon[1,2], Samir Brahim Belhaouari[3], Dalal Khalid Almutairi[4,*]

[1] *Basic Science Department, King Saud University, Saudi Arabia*
[2] *Department of Mathematics, Faculty of Science, Bakht Al-Ruda University, Sudan*
[3] *Division of Information and Computing Technology College of Science and Engineering, Hamad Bin Khalifa University, Qatar*
[4] *Department of Mathematics, College of Science Al-Zulfi, Majmaah University, Al-Majmaah 11952, Saudi Arabia*

Abstract. This work pioneers a novel approach in image edge detection through the utilization of the generalized fractional operator. By harnessing the global attributes inherent in fractional derivatives, it aims to enhance the extraction of intricate edge details.This is accomplished by creating the mask by using fractional derivative and adapt the mask by another parameter, yielding compelling and informative edge representations, as validated by experimental results. This advancement not only augments computer vision and image analysis techniques but also holds promise for refining image processing methodologies. Future endeavors may explore its adaptability across diverse imaging domains like medical and satellite imagery, while integration into deep learning frameworks could elevate its potential for advanced feature extraction and deeper image understanding. Additionally, optimizing its computational efficiency would broaden its scope for real-time deployment in fields such as robotics and autonomous systems.

2020 Mathematics Subject Classifications: 97M40, 65D18,97M40

Key Words and Phrases: Fractional-order, Edge detection, finite difference

---

1. Introduction

Edge detection is a foundational process in the realm of image processing, playing a pivotal role in various applications such as image segmentation, image compression, and image reconstruction [8, 13, 27, 32, 33, 44, 47]. Its primary objective is to pinpoint and delineate abrupt transitions in intensity or color within an image, often signifying object

*Corresponding author.
DOI: https://doi.org/10.29020/nybg.ejpam.v17i2.5141

Email addresses: dk.almutairi@mu.edu.sa (D. K. Almutairi), dbushra.c@ksu.edu.sa (D. E. Elgzouli), mabdoon.c@ksu.edu.sa (M. A. Abdoon), sbelhaouari@hbku.edu.qa (S. B. Belhaouari)

boundaries or other salient image features. Broadly categorized into two main methodologies, edge detection methods can be classified as either gradient-based or Laplacian-based [3, 7, 28, 29, 31, 35, 37, 39, 42, 43]

Gradient-based techniques identify edges by scrutinizing the gradient, or the first derivative, of the image. These methods aim to locate points in the image where intensity changes occur rapidly, typically marked by maximum or minimum values in the first derivative. However, one limitation of gradient-based approaches is their tendency to produce thicker edge representations, potentially leading to the loss of finer image details[6, 11, 34].

In contrast, generalized fractional Laplace operator concentrate on identifying zero-crossings in the fractional derivative.

These zero-crossings frequently coincide with the positions of edges. generalized fractional Laplace operator-based methods exhibit greater sensitivity to finer image details but may be more susceptible to the influence of noise in the image.

To tackle the challenge of striking a balance between edge thickness and noise sensitivity, fractional-order derivatives have been introduced[10, 18, 22]. Fractional derivatives expand upon the concept of integer derivatives, including first and second derivatives, by encompassing an infinite number of terms. This results in fractional derivatives serving as global operators, allowing them to consider information from a broader set of neighboring pixels. Consequently, fractional derivatives have the potential to retain more image edge details while ameliorating the effects of noise to some extent[5, 24, 45]. Significantly, researchers such as Pu et al. have proposed fractional differential masks designed to enhance image textures [17, 38, 41], and Bai and Feng have introduced fractional-order anisotropic diffusion models tailored for noise removal [26]. In this context, this paper introduces an innovative fractional-order Gr unwald-Letnikov operator with the specific aim of enhancing the structural features within an image, addressing the trade-off between edge thickness and sensitivity to noise. Experimental results showcase the promise of this operator in preserving image edge details, comparing favorably to traditional first-order and second-order Laplacian operators [30].

In comparison to other methods[23, 25, 36, 40, 46], the distinctiveness of this approach lies in its utilization of fractional derivatives and the development of a thresholding technique based on the mean fractional-order gradient, which collectively contribute to improved edge extraction and representation. The experimental validation further strengthens the credibility of the proposed method, suggesting its viability for practical applications in image processing and computer vision.

In summation, edge detection is a fundamental aspect of image processing, with the choice of method contingent on the specific application and the desired equilibrium between edge thickness and sensitivity to noise. Fractional-order derivatives present an intriguing avenue for achieving this equilibrium, with the proposed generalized fractional operator demonstrating substantial potential in safeguarding image edge details.

2. Basic Definitions and Tools

Definition 1[30]. Grünwald-Letnikov fractional derivative and integral definitions: Let α be any arbitrary positive real number, define α order derivative and α order integral of a continuous function f(x):

$$
\begin{aligned}
a^G D_x^\alpha f(x) &= \lim_{\substack{h\to 0\\ nh=x-a}} h^\alpha \sum_{k=0}^{\infty}(-1)^k \binom{\alpha}{k} f(x-kh)\\
&\text{and}\\
a^G D_x^{-\alpha} f(x) &= \lim_{\substack{h\to 0\\ nh=x-a}} h^\alpha \sum_{k=0}^{\infty} \binom{\alpha}{k} f(x-kh).
\end{aligned}
\tag{1}
$$

Riemann-Liouville fractional derivative and integral definitions [16]: Let m be positive integer, $n < \alpha < n+1$, define Riemann-Liouville α order derivative and α order integral of a continuous function f(x) :

$$
\begin{aligned}
a^R D_x^\alpha f(x) &= (\frac{d}{dt})^{n+1} \int_a^x (x-\tau)^{n-\alpha} f(\tau) d\tau.\\
&\text{and.}\\
a^R D_x^{-\alpha} f(x) &= \frac{1}{\Gamma n-\alpha} \int_a^x (x-\tau) f(\tau) d\tau.
\end{aligned}
\tag{2}
$$

vvvv

Define Liouville-Caputo fractional derivative and integral definitions[16]: Suppose that f(x) has morder continuous derivative, define Caputo's α order derivative and α order integral:

$$
\begin{aligned}
a^C D_x^\alpha f(x) &= \frac{1}{\Gamma(n-\alpha)} \int_a^x \frac{f^n(\tau)}{(x-\tau)^{\alpha+1-n}} d\tau, (n-1 \le \alpha \le n),\\
&\text{and.}\\
a^C D_x^\alpha f(x) &= \frac{1}{\Gamma(-\alpha)} \int_a^x (x-\tau)^{\alpha-1} f(\tau) d\tau.
\end{aligned}
\tag{3}
$$

Definition 2[20]. If f is a continuous function, then the generalized fractional integral denoted by $I_{a+}^{\alpha,\rho} f(x), \alpha > 0$, and $\rho > 0$, is given by the following:

$$
I_{a+}^{\alpha,\rho} f(x) = \frac{\rho^{1-\alpha}}{\Gamma(\alpha)} \int_a^x s^{\rho-1} \left(x^\rho - s^\rho\right)^{\alpha-1} f(s) ds, \alpha > 0, x > a.
$$

For $n-1 < \alpha \le n$ where $n \in \mathbb{N}$.

3. Edge Detection Operator

An essential area of image processing is edge detection. It contains methods for locating pixels in a digital image where the brightness intensity differs significantly from neighboring pixels. Numerous effective algorithms are suggested in the literature to identify edges. The majority of these algorithms are built using second-order differential operators, like the Laplace operator, and first-order operators, like the Sobel, Prewitt, and Roberts operators.

This feature might cause the matching masks to perform poorly in real-world applications. The performance of these algorithms to extract edges from images can also be hindered by noise [15, 19].

The Prewitt operator is a widely used filter for identifying an image's edges. The foundation of this strategy is the central difference is used to approximate the first-order derivative in this method. The image is convoluted using the following two kernels to obtain the method's results:

$\mathrm{h}_x =$

-1	0	1
-1	0	1
-1	0	1

$\mathrm{h}_y =$

-1	-1	-1
0	0	0
1	1	1

The Sobel operator, which is based on central finite differences, is another significant filter. In contrast to the Prewitt operator, the method's primary goal is to increase the number of partnerships with pixels that are closer to the mask's center. The following convolution kernels are employed in this method:

$\mathrm{f}_x =$

-1	0	1
-2	0	2
-1	0	1

$\mathrm{f}_y =$

-1	-2	-1
0	0	0
1	2	1

Although the Sobel operator will identify many false edges with a coarse edge width, it can also provide more accurate edge direction information. The Sobel operator is more sensitive to the diagonal edges than the horizontal and vertical edges, whereas the Prewitt operator is more sensitive to the horizontal and vertical edges. The integral differential operators of integer-order operators provide the foundation of each of the aforementioned kernels. Considering the notions of fractional difference has resulted in some significant advancements in this field. Fractional differential operators have produced amazing results in recent years when used to increase image quality, image texture enhancement, image noise reduction, and image edge analysis [4, 12]. One of the key equations for fractional differential operator expansion in images processing is to use the following general form:

$$D^{\alpha} f(s) \approx c_0 f(s) + c_1 f(s-1) + c_2 f(s-2) + c_3 f(s-3)..., \tag{4}$$

where the successive coefficients in the expansion of Eq.(4) are denoted by c1, c2, and c3.

In our method, we generalized the fractional operator in Eq.(4) to the new following operator

$$D^{\alpha,\rho}f(s) \approx c_0 f(s) + c_1 f(s-1) + c_2 f(s-2) + c_3 f(s-3).... \tag{5}$$

In light of this definition, the expansion can be extended in the following ways to the two-dimensional spaces of the images in the x and y directions:

$$\begin{aligned} D_x^{\alpha,\rho}f(x,y) &\approx c_0 f(x,y) + c_1 f(x-1,y) + c_2 f(x-2,y) + c_3 f(x-3,y)..., \\ D_y^{\alpha,\rho}f(x,y) &\approx c_0 f(x,y) + c_1 f(x,y-1) + c_2 f(x,y-2) + c_3 f(x,y-3).... \end{aligned} \tag{6}$$

In the remainder of the paper, the two structures in Eq.(5) will be used to make new fractional-order mask.

In this article, we build a 3 × 3 fractional integral mask by the following way:

$$\mathrm{f}_x = \begin{array}{|c|c|c|} \hline -c_0 & 0 & c_0 \\ \hline -c_1 & 0 & c_1 \\ \hline -c_2 & 0 & c_2 \\ \hline \end{array} \qquad \mathrm{f}_y = \begin{array}{|c|c|c|} \hline c_0 & c_1 & c_2 \\ \hline 0 & 0 & 0 \\ \hline -c_0 & -c_1 & -c_2 \\ \hline \end{array}$$

This kernel's design applies the vertical and horizontal pixels surrounding the central pixel. This kernel is a great tool for extracting texture and edges from images because of this important feature. Following the creation of these kernels, the gradient moduli are typically approximated as follows using the absolute values:
$|E|= |E_x|+|E_y|$
where:
$E_x = I(x,y) * f_x, \quad E_y = I(x,y) * f_y$
and I(x, y) is the pixel value of the gray scale image.

4. New edge detector based on Generalized Fractional-order.

The application of fractional-order derivative has been observed in various scientific domains see [41, 43], such as image processing.

To construct our method we approximate the fractional integral in definition (2) by the following way:

$$I_{a+}^{\alpha,\rho}f(x) = \frac{\rho^{1-\alpha}}{\Gamma(\alpha)} \int_a^x s^{\rho-1}\left(x^\rho - s^\rho\right)^{\alpha-1} f(s)ds, \alpha > 0, x > a. \tag{7}$$

let $f : [0,b] \to R$ and $I_{a+}^{\alpha,\rho}f$ is to be determined on $[0,b]$, choose $n+1$ grid points:
$0 = x_0 < x_1 < x_2... < x_n = b.$

We can define the function $f_n = [0, b] \to R$ using piecewise constant approach:

$$f_n(x) = f(x_j), \quad x \in [x_j, x_{j+1}]. \tag{8}$$

So we can uses $I_{a+}^{\alpha,\rho} f_n$ as an approximation for $I_{a+}^{\alpha,\rho} f$.
After doing some necessarily mathematical (see [12, 21])calculations finally we get the flowing formula:

$$I_{a+}^{\alpha,\rho} f(x_j) = \frac{h^\alpha \rho^{\alpha-2}}{\Gamma(\alpha+1)} \sum_{k=0}^{j-1} f(x_k)[(j^\rho - k^\rho)^\alpha - (j^\rho - (k+1)^\rho)^\alpha]. \tag{9}$$

where $h = \frac{b}{n}$ is equal step size in the grid $[x_j]$, $x_j = jh$.

Now we can using Eq.(9) to find the coefficients c_0, c_1, c_2 in Eq.(5) :

$$\begin{aligned}
I_{a+}^{\alpha,\rho} f(x_j) &= \frac{h^\alpha \rho^{\alpha-2}}{\Gamma(\alpha+1)}[(j^\rho - (j-1)^\rho)^\alpha] f(x_{j-1}) \\
I_{a+}^{\alpha,\rho} f(x_{j-1}) &= \frac{h^\alpha \rho^{\alpha-2}}{\Gamma(\alpha+1)}[((j-1)^\rho - (j-2)^\rho)^\alpha] f(x_{j-2}) \\
I_{a+}^{\alpha,\rho} f(x_{j-2}) &= \frac{h^\alpha \rho^{\alpha-2}}{\Gamma(\alpha+1)}[((j-2)^\rho - (j-3)^\rho)^\alpha] f(x_{j-2}).
\end{aligned} \tag{10}$$

Now, by taking $h = 1$ in Eq.(10) we obtain the following expansions:

$$\begin{aligned}
I_x^{\alpha,\rho} f(x,y) = &\frac{h^\alpha \rho^{\alpha-2}}{\Gamma(\alpha+1)}[(j^\rho - (j-1)^\rho)^\alpha] f(x,y) \\
&+ \frac{h^\alpha \rho^{\alpha-2}}{\Gamma(\alpha+1)}[((j-1)^\rho - (j-2)^\rho)^\alpha] f(x-1,y) \\
&+ \frac{h^\alpha \rho^{\alpha-2}}{\Gamma(\alpha+1)}[((j-2)^\rho - (j-3)^\rho)^\alpha] f(x-2,y),
\end{aligned} \tag{11}$$

$$\begin{aligned}
I_y^{\alpha,\rho} f(x,y) = &\frac{h^\alpha \rho^{\alpha-2}}{\Gamma(\alpha+1)}[(j^\rho - (j-1)^\rho)^\alpha] f(x,y) \\
&+ \frac{h^\alpha \rho^{\alpha-2}}{\Gamma(\alpha+1)}[((j-1)^\rho - (j-2)^\rho)^\alpha] f(x,y-1) \\
&+ \frac{h^\alpha \rho^{\alpha-2}}{\Gamma(\alpha+1)}[((j-2)^\rho - (j-3)^\rho)^\alpha] f(x,y-2).
\end{aligned} \tag{12}$$

Therefore, the coefficients for the Generalized Fractional-order are determined as follows:

$$
\begin{aligned}
c_0 &= \frac{h^\alpha \rho^{\alpha-2}}{\Gamma(\alpha+1)}[(j^\rho-(j-1)^\rho)^\alpha] \\
c_1 &= \frac{h^\alpha \rho^{\alpha-2}}{\Gamma(\alpha+1)}[((j-1)^\rho-(j-2)^\rho)^\alpha] \\
c_2 &= \frac{h^\alpha \rho^{\alpha-2}}{\Gamma(\alpha+1)}[((j-2)^\rho-(j-3)^\rho)^\alpha].
\end{aligned}
\tag{13}
$$

By using the obtained result in Eq.(13), the new mask taking the following form:

f_x=

$-\frac{\rho^{\alpha-2}}{\Gamma(\alpha+1)}[(j^\rho-(j-1)^\rho)^\alpha]$	0	$-\frac{\rho^{\alpha-2}}{\Gamma(\alpha+1)}[(j^\rho-(j-1)^\rho)^\alpha]$
$-\frac{\rho^{\alpha-2}}{\Gamma(\alpha+1)}[((j-1)^\rho-(j-2)^\rho)^\alpha]$	0	$-\frac{\rho^{\alpha-2}}{\Gamma(\alpha+1)}[((j-1)^\rho-(j-2)^\rho)^\alpha]$
$-\frac{\rho^{\alpha-2}}{\Gamma(\alpha+1)}[((j-2)^\rho-(j-3)^\rho)^\alpha]$	0	$-\frac{\rho^{\alpha-2}}{\Gamma(\alpha+1)}[((j-2)^\rho-(j-3)^\rho)^\alpha]$

f_y=

$\frac{\rho^{\alpha-2}}{\Gamma(\alpha+1)}$ $[(j^\rho-(j-1)^\rho)^\alpha]$	$\frac{\rho^{\alpha-2}}{\Gamma(\alpha+1)}$ $[((j-1)^\rho-(j-2)^\rho)^\alpha]$	$\frac{\rho^{\alpha-2}}{\Gamma(\alpha+1)}$ $[((j-2)^\rho-(j-3)^\rho)^\alpha]$
0	0	0
$-\frac{\rho^{\alpha-2}}{\Gamma(\alpha+1)}$ $[(j^\rho-(j-1)^\rho)^\alpha]$	$-\frac{\rho^{\alpha-2}}{\Gamma(\alpha+1)}$ $[((j-1)^\rho-(j-2)^\rho)^\alpha]$	$-\frac{\rho^{\alpha-2}}{\Gamma(\alpha+1)}$ $[((j-2)^\rho-(j-3)^\rho)^\alpha]$

The following table illustrate the algorithm for the new fractional edge detection.

	Algorithm: The edge detection using new generalized fractional operator
1	convert the input image to gray scale.
2	choose suitable $\alpha \in [0,1]$, and $\rho \geq 0$ to get the new fractional edge detector.
3	use Eq.(13) to obtain the new mask.

5. Experimental Work

The outcomes of edge identification in three photos collected using the Sobel, Prewitt, and generalized fractional edge detector techniques are covered in this section. The contrast, PSNR, and MSE values of each edge-detected image are then compared.

5.1. Edge detection

Edge detection is the process of identifying variations in intensity within an image field that are clearly distinct.

Edge detection uses sharp changes in intensity values at the object's two boundary areas to identify the object's edge. A group of connected pixels that define the boundary between two areas is called an edge. An edge contains important information that can be expressed by the object's dimensions or form. The gradient-based operator (first derivative), also known as the Sobel and Prewitt operators, is the first edge in some detector implementations.

5.2. Input image

Next, the MATLAB 2021 software is used to input the images that have been gathered for research. Table 1labels the images that were used in RGB color mode. The degree of difficulty associated with each image's edge detection determines which images are used as a dataset. In addition, the RGB color mode of the images is switched to gray scale.

sample-1	sample-2	sample-3
		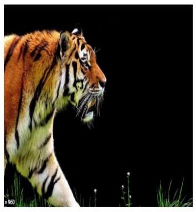

Table 1: Image samples

5.3. Image conversion and edge detection procedure

Technique for edge detection and image conversion. The image that was imported into the MATLAB application has now been converted to grayscale, as shown in Table 2.

This is necessary since the edge detection procedure can only be applied to images in grayscale color mode. After being converted to grayscale, the image moves on to the next stage, edge detection utilizing Sobel, Prewitt, and generalized fractional detector.

sample-1	sample-2	sample-3
		

Table 2: Grayscale images

5.4. Sobel operator

The first edge detection method, the sobel operator, requires first converting the image to grayscale in order to do edge detection.

5.5. Prewitt operator

In order to perform edge detection using the second edge detection technique, the Prewitt operator, the image must first be converted to grayscale. The code that uses the Prewitt operator to achieve edge detection after the convolution formula has been applied displays the edge detection image.

5.6. Generalized fractional operator

The third edge detection technique is the generalized fractional operator. After converting the original image to gray scale, edges are detected using the generalized fractional operator.

Fig.1a:Sobel mask.

Fig.1b: Prewitt mask.

Fig.1c:GF-at $\alpha = 0.35$,$\rho = 1$

Fig.1d: GF-at $\alpha = 0.35$, $\rho = 1.5$

Fig.1e: GF-at $\alpha = 0.35$, $\rho = 2$

Fig.1f: GF-at $\alpha = 0.40$, $\rho = 1$

Fig.1g: GF-at $\alpha = 0.40$ and $\rho = 1.5$

Fig.1h: GF-at$\alpha = 0.40$ and $\rho = 2$

Fig.2a:Sobel mask.

Fig.2b: Prewitt mask.

Fig.2c:GF-at$\alpha = 0.35$,$\rho = 1$

Fig.2d:GF-at $\alpha = 0.35$, $\rho = 1.5$

Fig.2e:GF-at $\alpha = 0.35$, $\rho = 2$

Fig.2f: GF-at $\alpha = 0.40$, $\rho = 1$

Fig.2g:GF-at $\alpha = 0.40$, $\rho = 1.5$

Fig.2h:GF-at $\alpha = 0.40$, $\rho = 2$

Fig.3a:Sobel mask.

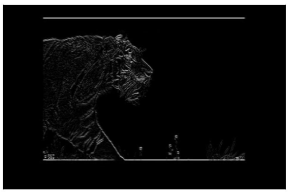

Fig.3b: Prewitt mask.

Fig.3c:GF-at $\alpha = 0.35$,$\rho = 1$

Fig.3d: GF-at $\alpha = 0.35$, $\rho = 1.5$

Fig.3e:GF-at $\alpha = 0.35$, $\rho = 2$

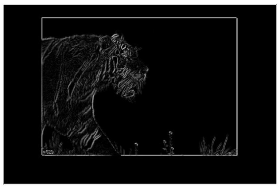

Fig.3f: GF-at$\alpha = 0.40$, $\rho = 1$

Fig.3g: GF-at $\alpha = 0.40$, $\rho = 1.5$

Fig.3h: GF-at $\alpha = 0.40$, $\rho = 2$

After successfully identifying the image's edges, a full complete discussion will be created for the previously results following the successful identification of the image's edges.

The MSE, PSNR, and contrast values are measured for all results are shown in Figs.1–3.

5.7. Calculation of MSE

Using the 24 binary images obtained from the edge detection process, the MSE was computed. The results from employing the four detection operators—Sobel, Prewitt and Generalized Fractional—to determine the MSE value of each edge-detected image are presented in Table3.

MSE values of sample-1-case-1			
$\alpha=\rho$ values	Sobel	Prewitt	G-F- method
$\alpha=0.35,\ \rho=1$	46409.129685	41860.148297	49443.110742
$\alpha=0.35,\ \rho=1.5$	46409.129685	41860.148297	40738.306791
$\alpha=0.35,\ \rho=2$	46409.129685	41860.148297	38375.214925
MSE values of sample-1-case-2			
$\alpha=0.40,\ \rho=1$	46409.129685	41860.148297	49560.930656
$\alpha=0.40,\ \rho=1.5$	46409.129685	41860.148297	41194.688260
$\alpha=0.40,\ \rho=2$	46409.129685	41860.148297	38784.421049
MSE values of sample-2-case-1			
$\alpha=\rho$ values	Sobel	Prewitt	G-F- method
$\alpha=0.35,\ \rho=1$	-44986.437879	38359.543095	49091.969362
$\alpha=0.35,\ \rho=1.5$	44986.437879	38359.543095	36823.880878
$\alpha=0.35,\ \rho=2$	44986.437879	38359.543095	33490.523683
MSE values of sample-2-case-2			
$\alpha=0.40,\ \rho=1$	44986.437879	38359.543095	49258.289239
$\alpha=0.40,\ \rho=1.5$	44986.437879	38359.543095	37474.303856
$\alpha=0.40,\ \rho=2$	44986.437879	38359.543095	34077.450522
MSE values of sample-3-case-1			
$\alpha=\rho$ values	Sobel	Prewitt	G-F- method
$\alpha=0.35,\ \rho=1$	46796.856189	40360.121740	51137.669257
$\alpha=0.35,\ \rho=1.5$	46796.856189	40360.121740	38921.258446
$\alpha=0.35,\ \rho=2$	46796.856189	40360.121740	35602.534842
MSE values of sample-3-case-2			
$\alpha=0.35,\ \rho=1$	46796.856189	40360.121740	51303.137432
$\alpha=0.35,\ \rho=1.5$	46796.856189	40360.121740	39565.565217
$\alpha=0.35,\ \rho=2$	46796.856189	40360.121740	36182.208594

Table 3: The MSE Results

5.8. Calculation of PSNR

After implementing edge detection to the four research material images, the next step is finding the PSNR value of the 24 binary images from the edge detection that completed in the first stage. Table 4 shows the outcomes of each edge-detected image's application of the three detection operators: Sobel, Prewitt and Generalized Fractional operator.

PSNR values of sample-1-case-1			
$\alpha = \rho$ values	Sobel	Prewitt	G-F- method
$\alpha = 0.35$, $\rho = 1$	-46.6660	-46.2180	-46.9411
$\alpha = 0.35$, $\rho = 1.5$	-46.6660	-46.2180	-46.1000
$\alpha = 0.35$, $\rho = 2$	-46.6660	-46.2180	-45.8405
PSNR values of sample-1-case-2			
$\alpha = 0.40$, $\rho = 1$	-46.6660	-46.2180	-46.9514
$\alpha = 0.40$, $\rho = 1.5$	-46.6660	-46.2180	-46.1484
$\alpha = 0.40$, $\rho = 2$	-46.6660	-46.2180	-45.8866
PSNR values of sample-2-case-1			
$\alpha = \rho$ values	Sobel	Prewitt	G-F- method
$\alpha = 0.35$, $\rho = 1$	-46.5308	-45.8387	-46.9101
$\alpha = 0.35$, $\rho = 1.5$	-46.5308	-45.8387	-45.6613
$\alpha = 0.35$, $\rho = 2$	-46.5308	-45.8387	-45.2492
PSNR values of sample-2-case-2			
$\alpha = 0.40$, $\rho = 1$	-46.5308	-45.8387	-46.9248
$\alpha = 0.40$, $\rho = 1.5$	-46.5308	-45.8387	-45.7373
$\alpha = 0.40$, $\rho = 2$	–46.5308	-45.8387	-45.3247
PSNR values of sample-3-case-1			
$\alpha = \rho$ values	Sobel	Prewitt	G-F- method
$\alpha = 0.35$, $\rho = 1$	-46.7022	-46.0595	-47.0874
$\alpha = 0.35$, $\rho = 1.5$	-46.7022	-46.0595	-45.9019
$\alpha = 0.35$, $\rho = 2$	-46.7022	-46.0595	-45.5148
PSNR values of sample-3-case-2			
$\alpha = 0.40$, $\rho = 1$	-46.7022	-46.0595	-47.1014
$\alpha = 0.40$, $\rho = 1.5$	-46.7022	-46.0595	-45.9732
$\alpha = 0.40$, $\rho = 2$	-46.7022	-46.0595	-45.5850

Table 4: The PSNR Results

5.9. Calculation of contrast

The contrast value of the image is evaluated via MATLAB's texture analysis feature. The outcomes of computing each image's contrast value after its edges were found using the Generalized Fractional, Prewitt, and Sobel detection operators are displayed in Table 5.

Contrast values of sample-1-case-1			
$\alpha=\rho$ values	Sobel	Prewitt	G-F- method
$\alpha=0.35,\ \rho=1$	2.3183	2.2535	4.0256
$\alpha=0.35,\ \rho=1.5$	2.3183	2.2535	3.7572
$\alpha=0.35,\ \rho=2$	2.3183	2.2535	3.6973
Contrast values of sample-1-case-2			
$\alpha=0.40,\ \rho=1$	2.3183	2.2535	4.0256
$\alpha=0.40,\ \rho=1.5$	2.3183	2.2535	3.7879
$\alpha=0.40,\ \rho=2$	2.3183	2.2535	3.7296
Contrast values of sample-2-case-1			
$\alpha=\rho$ values	Sobel	Prewitt	G-F- method
$\alpha=0.35,\ \rho=1$	4.3387	4.1220	6.1596
$\alpha=0.35,\ \rho=1.5$	4.3387	4.1220	5.9591
$\alpha=0.35,\ \rho=2$	-4.3387	4.1220	5.9107
Contrast values of sample-2-case-2			
$\alpha=0.40,\ \rho=1$	4.3387	4.1220	6.1596
$\alpha=0.40,\ \rho=1.5$	4.3387	4.1220	5.9795
$\alpha=0.40,\ \rho=2$	4.3387	4.1220	5.9488
Contrast values of sample-3-case-1			
$\alpha=\rho$ values	Sobel	Prewitt	G-F- method
$\alpha=0.35,\ \rho=1$	4.3387	4.1220	6.1596
$\alpha=0.35,\ \rho=1.5$	4.3387	4.1220	5.9591
$\alpha=0.35,\ \rho=2$	4.3387	4.1220	5.9107
Contrast values of sample-3-case-2			
$\alpha=0.40,\ \rho=1$	4.3387	4.1220	6.1596
$\alpha=0.40,\ \rho=1.5$	4.3387	4.1220	5.9795
$\alpha=0.40,\ \rho=2$	4.3387	4.1220	5.9488

Table 5: The Contrast Results

6. Performance Comparison

Various techniques such as Sobel, Prewitt, and Generalized Fractional operators can be used to identify edges in an image.

The edge detection quality analysis's results show that the Generalized Fractional operator produces the best edge detection, with an average PSNR value of -45.8405, according to the MSE, PSNR, and Contrast values on the Sobel, Prewitt, and Generalized Fractional operators. The average value of the Sobel and Prewitt operators is -46.6660 dB, -46.2180 dB, and -45.5148 dB, while the Sobel and Prewitt operators are -46.7022 dB, -46.0595 dB.

The Generalized Fractional operator has the lowest MSE value, 38375.214925, but the Sobel and Prewitt operators have average MSE values of 46409.129685 and 41860.148297, respectively. The operator with the highest average score, 5.9488, is the Generalized Fractional operator operator, according on the comparison of Contrast values.

However, the Contrast setting just serves as a supporting parameter to draw attention to the differences in the output of each edge detection operator.

7. Conclusion

This work pioneers a novel approach in image edge detection through the utilization of the Generalized Fractional. By harnessing the global attributes inherent in fractional derivatives, it aims to enhance the extraction of intricate edge details.This is accomplished by creating the mask by using fractional derivative and adapt the mask by another parameter, yielding compelling and informative edge representations. Given that the Generalized Fractional edge detection approach has the lowest MSE value and the highest PSNR and Contrast value among the other two ways, it can be argued that it is the best method. This advancement not only augments computer vision and image analysis techniques but also holds promise for refining image processing methodologies. Future endeavors may explore its adaptability across diverse imaging domains like medical and satellite imagery, while integration into deep learning frameworks could elevate its potential for advanced feature extraction and deeper image understanding. Additionally, optimizing its computational efficiency would broaden its scope for real-time deployment in fields such as robotics and autonomous systems. Future research could extend its use to various imaging domains, integrate it into deep learning for advanced analysis, and optimize its efficiency for real-time applications in robotics and autonomous systems . Further exploration might involve applying this technique to new fractional models and comparing its effectiveness with existing numerical methods [1, 2, 9, 14].

Acknowledgements

The authors extend their appreciation to the Deanship of Postgraduate Studies and Scientific Research at Majmaah University for funding this research work.

References

[1] Abdulrahman BM Alzahrani, Mohamed A Abdoon, Mohamed Elbadri, Mohammed Berir, and Diaa Eldin Elgezouli. A comparative numerical study of the symmetry chaotic jerk system with a hyperbolic sine function via two different methods. *Symmetry*, 15(11):1991, 2023.

[2] Abdulrahman BM Alzahrani, Rania Saadeh, Mohamed A Abdoon, Mohamed Elbadri, Mohammed Berir, and Ahmad Qazza. Effective methods for numerical analysis of the simplest chaotic circuit model with atangana–baleanu caputo fractional derivative. *Journal of Engineering Mathematics*, 144(1):9, 2024.

[3] Ghassan Mahmoud Husien Amer and Ahmed Mohamed Abushaala. Edge detection methods. In *2015 2nd World Symposium on Web Applications and Networking (WSWAN)*, pages 1–7. IEEE, 2015.

[4] Saeed Balochian and Hossein Baloochian. Edge detection on noisy images using prewitt operator and fractional order differentiation. *Multimedia Tools and Applications*, 81(7):9759–9770, 2022.

[5] Huaiguang Chen, Haili Qiao, Wenyu Wei, and Jin Li. Time fractional diffusion equation based on caputo fractional derivative for image denoising. *Optics & Laser Technology*, 168:109855, 2024.

[6] William Chen. *Applications of Large Language Models for Robot Navigation and Scene Understanding.* PhD thesis, Massachusetts Institute of Technology, 2023.

[7] Vikram Mutneja Dharampal. Methods of image edge detection: A review. *J. Electr. Electron. Syst*, 4(2):2332–0796, 2015.

[8] Sachin Dhawan. A review of image compression and comparison of its algorithms. *International Journal of electronics & Communication technology*, 2(1):22–26, 2011.

[9] Mohamed Elbadri, Mohamed A Abdoon, Mohammed Berir, and Dalal Khalid Almutairi. A numerical solution and comparative study of the symmetric rossler attractor with the generalized caputo fractional derivative via two different methods. *Mathematics*, 11(13):2997, 2023.

[10] Mohamed Elbadri, Mohamed A Abdoon, Mohammed Berir, and Dalal Khalid Almutairi. A symmetry chaotic model with fractional derivative order via two different methods. *Symmetry*, 15(6):1151, 2023.

[11] Mathieu Even, Scott Pesme, Suriya Gunasekar, and Nicolas Flammarion. (s) gd over diagonal linear networks: Implicit bias, large stepsizes and edge of stability. In *Thirty-seventh Conference on Neural Information Processing Systems*, 2023.

[12] Behzad Ghanbari and Abdon Atangana. Some new edge detecting techniques based on fractional derivatives with non-local and non-singular kernels. *Advances in Difference Equations*, 2020(1):1–19, 2020.

[13] Wesley Grignani, Douglas Almeida dos Santos, Luigi Dilillo, Felipe Viel, and Douglas Rossi de Melo. A low-cost hardware accelerator for ccsds 123 lossless hyperspectral image compression. In *DFT 2023-36th IEEE International Symposium on Defect and Fault Tolerance in VLSI and Nanotechnology Systems*, 2023.

[14] Fathelrhman EL Guma, Ossama M Badawy, Mohammed Berir, and Mohamed A Abdoon. Numerical analysis of fractional-order dynamic dengue disease epidemic in sudan. *Journal of the Nigerian Society of Physical Sciences*, pages 1464–1464, 2023.

[15] Lili Han, Yimin Tian, and Qianhui Qi. Research on edge detection algorithm based on improved sobel operator. In *MATEC Web of Conferences*, volume 309, page 03031. EDP Sciences, 2020.

[16] Rudolf Hilfer, Yury Luchko, and Zivorad Tomovski. Operational method for the solution of fractional differential equations with generalized riemann-liouville fractional derivatives. *Fract. Calc. Appl. Anal*, 12(3):299–318, 2009.

[17] Tingsheng Huang, Xinjian Wang, Da Xie, Chunyang Wang, and Xuelian Liu. Depth image enhancement algorithm based on fractional differentiation. *Fractal and Fractional*, 7(5):394, 2023.

[18] Samar M Ismail, Lobna A Said, Ahmed G Radwan, Ahmed H Madian, and Mohamed F Abu-ElYazeed. A novel image encryption system merging fractional-order edge detection and generalized chaotic maps. *Signal Processing*, 167:107280, 2020.

[19] T Jagadesh. Implementation of prewitt operator based edge detection algorithm using fpga.

[20] Udita N Katugampola. Existence and uniqueness results for a class of generalized fractional differential equations. *arXiv preprint arXiv:1411.5229*, 2014.

[21] Kamlesh Kumar, Rajesh K Pandey, and Shiva Sharma. Approximations of fractional integrals and caputo derivatives with application in solving abel's integral equations. *Journal of King Saud University-Science*, 31(4):692–700, 2019.

[22] Die Li, Chunna Zhao, Murong Jiang, Yaqun Huang, and Yinghua Li. Fractional order edge detection method. In *2019 IEEE 11th International Conference on Communication Software and Networks (ICCSN)*, pages 529–534. IEEE, 2019.

[23] Zhen Li. Edge detection algorithm in complex image text information extraction. *Journal of Computational Methods in Sciences and Engineering*, (Preprint):1–13, 2023.

[24] Xing-ran Liao. An improved rof denoising model based on time-fractional derivative. *Frontiers of Information Technology & Electronic Engineering*, 21(6):856–865, 2020.

[25] Dujin Liu, Shiji Zhou, Rong Shen, and Xuegang Luo. Color image edge detection method based on the improved whale optimization algorithm. *IEEE Access*, 11:5981–5989, 2023.

[26] Barbara Lupinska. Properties of the katugampola fractional operators. *Tatra Mt. Math. Publ*, 79:135–148, 2021.

[27] Shervin Minaee, Yuri Boykov, Fatih Porikli, Antonio Plaza, Nasser Kehtarnavaz, and Demetri Terzopoulos. Image segmentation using deep learning: A survey. *IEEE transactions on pattern analysis and machine intelligence*, 44(7):3523–3542, 2021.

[28] Phillip A Mlsna and Jeffrey J Rodriguez. Gradient and laplacian edge detection. In *The essential guide to image processing*, pages 495–524. Elsevier, 2009.

[29] S Nashat, A Abdullah, and MZ Abdullah. Unimodal thresholding for laplacian-based canny–deriche filter. *Pattern Recognition Letters*, 33(10):1269–1286, 2012.

[30] Manuel Duarte Ortigueira and Fernando Coito. From differences to derivatives. *Fractional Calculus and Applied Analysis*, 7(4):459, 2004.

[31] Mohammadreza Asghari Oskoei and Huosheng Hu. A survey on edge detection methods. *University of Essex, UK*, 33, 2010.

[32] Yun Ouyang and Wusheng Wang. Comparison of definition of several fractional derivatives. In *2016 International Conference on Education, Management and Computer Science*, pages 553–557. Atlantis Press, 2016.

[33] Sung Cheol Park, Min Kyu Park, and Moon Gi Kang. Super-resolution image reconstruction: a technical overview. *IEEE signal processing magazine*, 20(3):21–36, 2003.

[34] Max Schwarzer, Johan Samir Obando Ceron, Aaron Courville, Marc G Bellemare, Rishabh Agarwal, and Pablo Samuel Castro. Bigger, better, faster: Human-level atari with human-level efficiency. In *International Conference on Machine Learning*, pages 30365–30380. PMLR, 2023.

[35] Bickey Kumar Shah, Vansh Kedia, Rohan Raut, Sakil Ansari, and Anshul Shroff. Evaluation and comparative study of edge detection techniques. *IOSR Journal of Computer Engineering*, 22(5):6–15, 2020.

[36] Hossein Shahverdi, Mohammad Nabati, Parisa Fard Moshiri, Reza Asvadi, and Seyed Ali Ghorashi. Enhancing csi-based human activity recognition by edge detection techniques. *Information*, 14(7):404, 2023.

[37] GT Shrivakshan and Chandramouli Chandrasekar. A comparison of various edge detection techniques used in image processing. *International Journal of Computer Science Issues (IJCSI)*, 9(5):269, 2012.

[38] Anil K Shukla, Rajesh K Pandey, and Swati Yadav. Adaptive fractional masks and super resolution based approach for image enhancement. *Multimedia Tools and Applications*, 80(20):30213–30236, 2021.

[39] Simranjit Singh and Rakesh Singh. Comparison of various edge detection techniques. In *2015 2nd International Conference on Computing for Sustainable Global Development (INDIACom)*, pages 393–396. IEEE, 2015.

[40] Jibi G Thanikkal, Ashwani Kumar Dubey, and MT Thomas. A novel edge detection method for medicinal plant's leaf features extraction. *International Journal of System Assurance Engineering and Management*, 14(1):448–458, 2023.

[41] Dan Tian, Jing Fei Wu, and Ya Jie Yang. A fractional-order laplacian operator for image edge detection. *Applied Mechanics and Materials*, 536:55–58, 2014.

[42] Huilin Xu and Yuhui Xiao. A novel edge detection method based on the regularized laplacian operation. *Symmetry*, 10(12):697, 2018.

[43] Charles Yaacoub and Roy Abi Zeid Daou. Fractional order sobel edge detector. In *2019 Ninth International Conference on Image Processing Theory, Tools and Applications (IPTA)*, pages 1–5. IEEE, 2019.

[44] Shimon D Yanowitz and Alfred M Bruckstein. A new method for image segmentation. *Computer Vision, Graphics, and Image Processing*, 46(1):82–95, 1989.

[45] Xuehui Yin, Shangbo Zhou, et al. Image structure-preserving denoising based on difference curvature driven fractional nonlinear diffusion. *Mathematical Problems in Engineering*, 2015, 2015.

[46] Ri-Gui Zhou, Han Yu, Yu Cheng, and Feng-Xin Li. Quantum image edge extraction based on improved prewitt operator. *Quantum Information Processing*, 18:1–24, 2019.

[47] Zeyu Zhou, Abdulrahman Alfayad, Tzu Cheng Chao, and James G Pipe. Acoustic noise reduction for spiral mri by gradient derating. *Magnetic Resonance in Medicine*, 2023.